Catalysis Communications 36 (2013) 10–15

Contents lists available at SciVerse ScienceDirect

Catalysis Communications

journal homepage: www.elsevier.com/locate/catcom

Short Communication

Effect of the cerium loading on the HMS structure. Preparation, characterization and catalytic properties

Maria Luisa Saladino [a,*], Delia F. Chillura Martino [b], Elka Kraleva [c], Eugenio Caponetti [a,b]

[a] Centro Grandi Apparecchiature-UniNetLab, Università di Palermo, Via Marini 14, Palermo I-90128, Italy
[b] Dipartimento di Scienze e Tecnologie Biologiche Chimiche e Farmaceutiche and INSTM UdR - Palermo, Università di Palermo, Parco d'Orleans II, Viale delle Scienze pad.17, Palermo 90128, Italy
[c] Leibniz Institute for Catalysis, University of Rostock (LIKAT), Albert-Einstein-Str. 29 a, D-18059 Rostock, Germany

ARTICLE INFO

Article history:
Received 20 December 2012
Received in revised form 20 February 2013
Accepted 22 February 2013
Available online 4 March 2013

Keywords:
Mesoporous
HMS
Cerianite
Catalytic evaluation

ABSTRACT

Ce–HMS mesoporous materials were prepared by incipient wetness method starting from HMS synthesized in acid condition. The effect of cerium quantity, in the range of Ce/Si atomic ratio 0.02–0.3, on its structure and properties was investigated. Results showed that the HMS hexagonal structure was maintained after the cerium adding. Furthermore, the surface area and the pore volume were reduced. The presence of the *cerianite* nanoparticles located within the HMS channels up to 0.05, thus covering the HMS surface at higher Ce/Si atomic ratio, was observed. The catalytic performances of the materials were tested in ethanol partial oxidation reaction.

1. Introduction

Since it was first reported by Mobil Company in 1992 [1], mesoporous materials, such as MCM-41, SBA-15 and hexagonal mesoporous silica (HMS), play a significant role in several fields such as adsorption, medication, catalysis, etc. Their high specific surface area and tuneable pore size make them very attractive supports; in fact, they are capable of holding metal oxides in nanodimensions that, due to interactions with the host structure, can infer redox and acid catalytic properties and high catalytic activity [2–4].

In catalysis the rare earths were mainly used as promoters but can be used as the active components of catalyst in the oxides or in the microporous materials [5, 6]. In particular, cerium containing MCM-41 material has been used for many catalytic applications [7, 8]. The cerium incorporation into the mesoporous silica network or the adding of its oxides on the surface makes a mesoporous material a bifunctional catalyst in heterogeneous acid as well as redox catalysis.

Catalyst precursor, support, preparation method and metal loading can influence the behavior of cerium catalysts [9]. Most of the papers report the incorporation of cerium in the MCM-41 framework during the synthesis. At our knowledge, only few papers report the adding of cerium oxides on the surface [10].

Partial oxidation is a very interesting process for hydrogen production because the system can be auto-thermally run, thereby eliminating the need for external heat. Moreover, it is much faster than catalytic steam reforming, which allows a quick start-up and short response times. Ethanol partial oxidation follows a very complex pathway, including several reaction intermediates formed and decomposed on both, the supports and active metals, making up the catalytic systems. The nature of the support directly influences the product distribution and catalyst stability during ethanol conversion reactions [11, 12]. Several active phases have been proposed to serve as a good supports of catalyst for this reaction [13–15]. Since HMS exhibits high surface area and highly ordered mesopores in the range 20–100 Å, the synthesis of Ce containing HMS mesoporous materials will definitively open up a new possibility for the catalysts with uniform pores in the mesoporous region so that large molecules can freely diffuse through their pores [16].

In this paper, the preparation of a new material, the Ce–HMS, is reported. HMS was synthesized in acid conditions, and then, the cerium oxide was added by using the incipient wetness method. Small angle X-ray scattering, X-ray diffraction, N_2 adsorption and ^{29}Si Cross Polarization–Magic Angle Spinning NMR are carried out to investigate the effect of cerium/silica molar ratio on the characteristics of mesoporous Ce–HMS. Finally, the catalytic activity of the prepared samples was evaluated in the bio-ethanol partial oxidation reaction.

* Corresponding author. Tel.: +39 091 23897921; fax: +39 091 590015.
E-mail address: marialuisa.saladino@unipa.it (M.L. Saladino).

1566-7367/$ – see front matter
http://dx.doi.org/10.1016/j.catcom.2013.02.023

2. Experimental section

2.1. Materials

Cetyltrimetylammonium bromide (CTAB, Aldrich), cerium nitrate esahydrate (Aldrich), hydrochloric acid (Aldrich, 37%), and tetraethoxysilane (TEOS, Fluka) were used as received. Solutions were prepared by weight adding conductivity grade water.

2.2. Sample preparation

2.2.1. HMS

Mesoporous silica was prepared by adding the silica precursor tetraethoxysilane to an aqueous solution containing cetyltrimethylammonium bromide (CTAB) as template in acid environment. The reactants molar ratios were: $CTAB/SiO_2 = 0.21$, $HCl/SiO_2 = 2.1$ and $H_2O/SiO_2 = 146$. The obtained precipitate was recovered after 2 h by filtration, washed, dried at room temperature and calcined on air at 600 °C for 4 h.

2.2.2. Ce–HMS

Five samples with Ce/Si atomic ratio *R* equal to 0.02, 0.05, 0.1, 0.2, and 0.3 were prepared by impregnation. Calcined mesoporous silica samples were treated with ethanol solutions containing the adequate amounts of cerium nitrate, following the incipient wetness method [17]. Samples were treated for 24 h at 60 °C in order to move away the ethanol. The dry materials were thermally treated at 350 °C for 1 h and, then, at 400 °C for 2 h. At the end of the impregnation process the material color changed from white to yellow wherein its intensity depends on cerium loading. An aliquot of non-impregnated HMS was treated at the same conditions in order to be used as *reference* sample ($R = 0$).

2.3. Characterization methods

Small Angle X-ray Scattering measurements were taken using a Bruker AXS Nanostar-U instrument wherein its source was a Cu rotating anode working at 40 kV and 18 mA. The X-ray beam was monochromatized at a wavelength λ of 1.54 Å (Cu Kα) using a couple of Göbel mirrors and was collimated using three pinholes with diameters of 500, 150 and 500 μm. Samples were directly mounted on the sample stage to avoid additional scattering of the holder. Data were collected at room temperature for 1000 s, and were recorded in a two-dimensional multiwire proportional counter detector placed at 24 cm from the sample. The measurements were carried out in two different portions of each sample to check its homogeneity.

X-ray diffraction (XRD) patterns were recorded with a Phylips diffractometer in the Bragg–Brentano geometry using a Ni filtered Cu Kα radiation (λ = 1.54056 Å) and a graphite monochromator in the diffracted beam. The X-ray generator worked at 40 kV and 30 mA; the instrument resolution (divergent and antiscatter slits of 0.5°) was determined using standards free from the effect of reduced crystallite size and lattice defects. The diffraction patterns were analyzed according to the Rietveld method [18] using the program MAUD [19].

N_2 absorption–desorption isotherms were registered at 77 K using a Quantachrome Nova 2200 Multi-Station High Speed Gas Sorption Analyzer. Samples were outgassed for 3 h at 573 K in the degas station. Adsorbed nitrogen volumes were normalized to the standard temperature and pressure.

^{13}C Cross Polarization–Magic Angle Spinning Nuclear Magnetic Resonance (^{13}C {^1H} CP–MAS NMR) spectra were obtained at room temperature through a Bruker Avance II 400 MHz (9.4 T) spectrometer operating at 79.4 MHz for the ^{29}Si nucleus with MAS rate of 5 kHz, 4096 scans, contact time of 8 ms and repetition delay of 8 s. The optimization of the Hartmann–Hahn condition [20] was obtained using a Q_8M_8 ($Si[(CH_3)_3]_8Si_8O_{20}$) standard. All samples were placed in a 4 mm zirconia rotor sealed with KEL-F caps.

2.4. Catalytic test

The obtained materials were tested in the bio-ethanol partial oxidation reaction as a probe reaction.

The experiments were carried out in a fixed bed reactor at atmospheric pressure and a temperature of the reactor furnace between 400 and 600 °C in order to avoid thermal hot spot effect in catalytic levels determined real maximal temperature around 700 °C [21]. This effect, described by W.Wang et al. [22], is due to the overall exothermic nature of reactions contributing to the catalytic partial oxidation of ethanol. Typically, around 150 mg of each sample was mixed with silica as an inert material in a ratio of 1/10. The catalytic test was carried out using a constant feed composition with an oxygen:ethanol molar ratio of 0.75. Environmentally sustainable bio-ethanol (Richter GmbH) with 96.6% purity was used as fuel. A constant bio-ethanol flow rate of 10 g/h was evaporated at 120 °C and then mixed with a gas stream of Air (291 ml/min) and nitrogen (100 ml/min). The nitrogen was used as the inert component as a balance. Space velocity (GHSV), defined as the ratio of the total volumetric flow at reaction conditions to the catalytic volume, was 35,000 h^{-1}. Composition of the inlet and outlet gases was analyzed on-line using a *Shimadzu* gas chromatograph equipped with FID and TCD detectors at λ = 0.25 nm. The carbon balance was around 100% for all samples. To evaluate catalyst performance, the following parameters were calculated:

$$\text{Conversion of ethanol } X_{Ethanol}(\%) = \frac{F_{Ethanol\_in} - F_{Ethanol\_out}}{F_{Ethanol\_in}} \times 100$$

$$\text{Selectivity to hydrogen } S_{H_2}(\%) = \frac{F_{H_2}}{n_i \times (F_{Ethanol\_in} - F_{Ethanol\_out})} \times 100$$

$$\text{Selectivity to carbon-containing products } S_i(\%) = \frac{F_{carbon-containing\_products}}{n_i \times (F_{Ethanol\_in} - F_{Ethanol\_out})} \times 100$$

where F_{i_in} and F_{i_out} are the molar flow of the *i* species at the inlet and outlet of the reactor respectively, and n_i is the stoichiometric factor between the carbon-containing products and ethanol. The quantity of water in the system was not calculated because of working in a dry base in gas phase.

3. Results and discussion

3.1. Structural characterization

The SAXS two-dimensional patterns of HMS and of Ce–HMS samples were isotropic. They were averaged around annular rings, thus providing the scattering intensity *I(Q)* in the 0.02–0.8 $Å^{-1}Q$ range. Q, the momentum transfer, is equal to $4\pi\sin\theta/\lambda$, being 2θ the scattering angle. Measurements, carried out on different portions of the samples, were overlapped thus showing that samples are homogeneous. SAXS data of Ce–HMS samples, after correction for the background, are reported versus 2θ in Fig. 1.

The presence of a strong diffraction peak around $2\theta = 2.8°$ is a characteristic of the (1 0 0) plane for the hexagonal lattice, typical of HMS [23]. The peak is also present in the impregnated samples at low cerium amount indicating that the pore structure of HMS was not modified as a consequence of the impregnation. However, by increasing the cerium amount a decrease of the intensity and a small shift of the peak were observed which indicates a disordering of the hexagonal arrangement of pores.

The interplanar distance in the (1 0 0) direction, d_{100}, was calculated by Bragg's Law ($\lambda = 2d_{hkl}\sin\theta$) and the unit cell parameter 'a_0', indicating the distance between the center of two adjacent pores in the

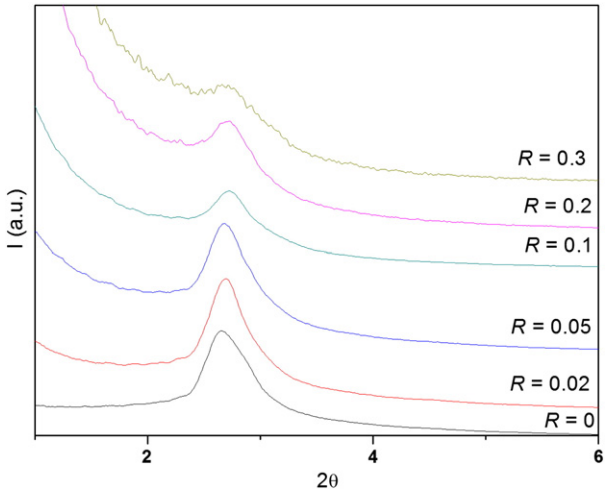

Fig. 1. SAXS intensities vs. 2θ of Ce–HMS samples with different *R*.

hexagonal structure, was obtained as $a_0 = 2d_{100} / \sqrt{3}$. For each sample, the calculated a_0 values are reported inTable 1.

After calcination, the hexagonal unit cell parameter, *a*, slightly decreases up to $R = 0.1$, thus, remaining constant at higher molar ratio.

XRD diffraction patterns of Ce–HMS samples are reported in Fig. 2.

The XRD pattern of HMS ($R = 0$) shows the characteristic large band among 20–30°, ascribed to the amorphous SiO_2 which is not organized to the HMS structure. The XRD patterns of Ce–HMS samples show the peaks of crystalline phases superimposed to the amorphous band. The peaks correspond to the CeO_2 cubic phase of *cerianite*, (space group Fm-3m, lattice parameters $a = b = c = 5.417$ Å, $\alpha = \beta = \gamma = 90°$). However, the peak profile is very broad thus suggesting the presence of nanoparticles and a lattice large disorder. The intensity of the crystalline phases increases and the peak broadening decreases with the cerium loading.

The diffraction patterns were analyzed using the Rietveld method [18]. In order to obtain the structural parameters of cerianite, for each pattern the contribute of the amorphous band was subtracted to the patterns. As an example, the bar sequence of the cerianite reference diffraction pattern and the curve of residues computed by the Rietveld best fit on Ce–HMS with $R = 0.02$ and 0.3 are shown at the bottom of Fig. 2B and C, respectively. Lines superimposed to the experimental patterns are the result of the best fit. The agreement between the computed intensity and experimental data is fairly good in every case.

For each sample the cell parameter, *a*, the average crystallite size, D, and the lattice disorder, ε, are reported in Table 1.

The pattern analysis showed that the lattice parameter of cerianite in the samples loaded with lower quantity is slightly different to the ones reported in literature. The difference is due to the small quantities of cerianite present in the sample and its small crystallite size which gives a very small contribute to the XRD pattern hidden by the large band of the amorphous. The lattice parameter values of cerianite of the other samples are similar to the literature value.

Table 1
Structural data of Ce–HMS samples.

Sample	*R*	α_0 (Å)	*a* (Å)	D (Å)	ε
HMS	0	38.5(1)	–	–	–
Ce–HMS	0.02	38.2(1)	5.446(2)	26(5)	$1.6 \cdot 10^{-2}$
Ce–HMS	0.05	38.0(1)	5.411(2)	58(3)	$1.2 \cdot 10^{-2}$
Ce–HMS	0.1	37.3(1)	5.425(2)	57(3)	$1.3 \cdot 10^{-2}$
Ce–HMS	0.2	37.3(1)	5.422(2)	51(2)	$1.0 \cdot 10^{-2}$
Ce–HMS	0.3	37.3(1)	5.426(2)	50(2)	$1.0 \cdot 10^{-3}$

α_0: distance between the center of two adjacent pores in the hexagonal structure; *a*: cell parameter of cerianite; D: average crystallite size of cerianite; ε: lattice disorder of cerianite phase. The uncertainty on the values is in parenthesis.

The average crystallite size, D, corresponding to the average coherent diffraction domain, was calculated after separating strain from size effects according to the Rietveld approach [18] using the isotropic model, which can be regarded as a first approximation for a volume weighted average size of crystallites, regardless their shape and texture. As expected, the D value increases with the cerium loading (from to 26 to 50 Å). The lattice disorder (microstrain, ε) of the cerianite decreases with the cerium amount.

Nitrogen adsorption–desorption isotherms were registered to obtain information about the surface area and the pore size and some of them are reported in Fig. 3. According to IUPAC [24] the characteristic type IV-isotherms for mesoporous HMS are obtained. Three well-defined stages may be identified: (1) a slow increase in nitrogen uptake at low relative pressure, corresponding to a monolayer-multilayer adsorption on the pore walls; (2) a sharp step at intermediate relative pressures indicative of a capillary condensation within mesopores; and (3) a plateau with a slight inclination at high relative pressures associated with a multilayer adsorption on the external surface of the crystals.

The nitrogen adsorption–desorption isotherms of Ce–HMS do not change significantly up to *R* equal to 0.3. The specific surface area (S_{BET}) was calculated according to the standard BET method [25] in the relative adsorption pressure (P/P_0) range from 0.045 to 0.250. The total pore volume (V_t) was obtained from the nitrogen amount adsorbed in correspondence of P/P_0 equal to 0.99. The cylinder diameter size (w_{BJH}) was calculated by the BJH method [26]. The pore wall thickness (t) was then estimated as $t = a_0 - k\, w_{BJH}$, where k is a constant that for hexagonal cylinder and pore wall mass density was obtained by using geometrical consideration equal to 0.95 [27]. S_{BET}, V_t, w_{BJH} and the *t* values are reported in Fig. 3, as function of *R*.

By increasing the cerium quantity, S_{BET}, Vt, and w_{BJH} decrease, while the pore wall thickness *t*, estimated on the basis of Eq. (2), increases.

These findings indicate that during the impregnation process the ethanol solution containing Ce(III) ions diffuse into the pores. After the ethanol removal the thermal treatment causes the oxidation of the Ce(III) to Ce(IV) and the formation of CeO_2 nanoparticles which remain trapped thus increasing the wall thickness and partially obstructing the mesochannels.

Comparing the obtained D and w_{BJH} values for each sample, it is possible to assert that in Ce–HMS with $R = 0.02$ the cerianite nanoparticles are inside the mesochannels. In the other samples the D value is higher than w_{BJH}, thus suggesting that the most of cerianite particles are on the surface of the material. This finding also explains the observed difference in the cell parameter of cerianite in the sample with $R = 0.02$. Due to the surface area decrease it is not possible to exclude the presence of cerianite also inside the channels.

The $^{29}Si\{^1H\}$ CP–MAS NMR spectra of Ce–HMS samples are reported in Fig. 4A.

It is well known that the $^{29}Si\{^1H\}$ CP–MAS NMR spectrum of HMS of Fig. 4A is due to the contribution of the three peaks: the first peak, Q2, centered at around −90 ppm, is attributed to the geminal silanols, the second peak, Q3, at around −100 ppm, is attributed to the silicon atoms bearing one hydroxyl group and the third peak, Q4, at around −109 ppm, is attributed to the silicon atoms without hydroxyl groups [17].

Since the $^{29}Si\{^1H\}$ CP–MAS NMR technique is based on the magnetization transfer from ^1H to ^{29}Si nuclei, the peak intensities are related to the total number of protons near the silicon atoms. As a consequence a straight quantification of the different silicon groups is not possible. However, as the bare and the functionalized HMS spectra show the same chemical shifts and the same cross polarization dynamic, the relative intensities of the three different silicon contributions in the samples are still reliable because the variation of the contact time does not modify the relative intensity distribution of the signals. Then, the deconvolution of each spectrum has been performed to calculate the single contributions of the three signals.

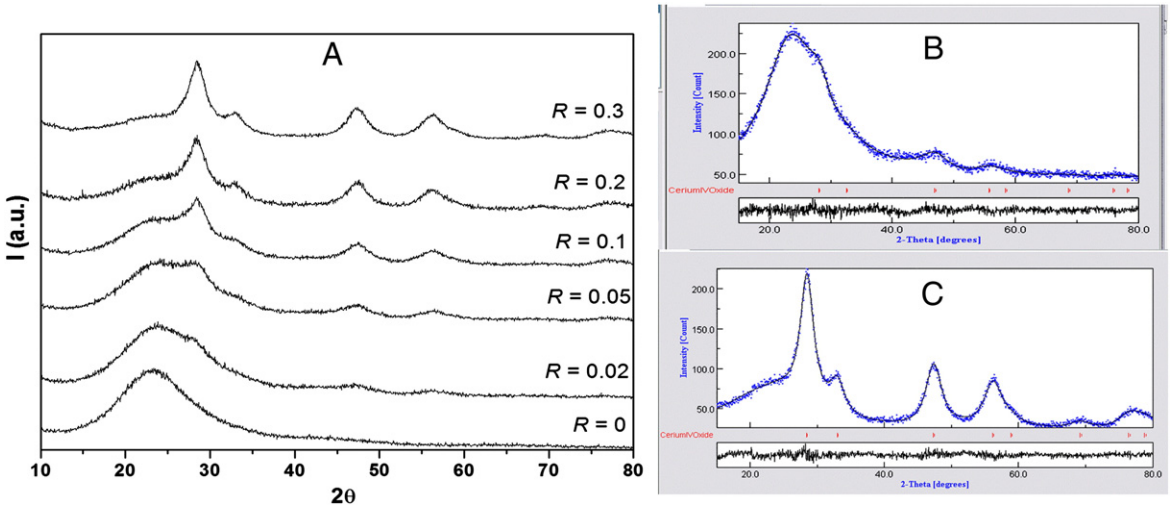

Fig. 2. A) XRD patterns of Ce–HMS samples with different *R*; B and C) Rietveld analysis diffraction patterns of Ce–HMS with $R = 0.02$ and $R = 0.3$, respectively. XRD experimental patterns (dots) and Rietveld fits (full lines). The bar sequence of reference diffraction pattern and a curve of residuals are shown along the bottom.

The relative values are reported in Fig. 4B. A decrease of $(Si–O)_3–Si–OH$ groups together with an increase of $Si–(Si–O)_4$ groups was observed up to $R = 0.05$. At higher *R* the Q2, Q3 and Q4 values do not significantly change. In addition, the $Q4/(Q2 + Q3)$ ratio, which could be taken as a measure of the link between Ce ions and the silica surface, is reported in Fig. 4C as function of *R*. The $Q4/(Q2 + Q3)$ ratio increases with the cerium quantity up to reach a plateau. Results can be explained considering the formation of a link between cerium and the HMS silica surface as a consequence of the impregnation process. At $R = 0.05$ the HMS surface is totally covered by cerianite, according to the XRD and isotherms data analysis.

3.2. Catalytic performance

The partial oxidation reaction of ethanol was carried out in absence of catalyst and in presence of Ce–HMS samples working at same conditions. Experiments were conducted twice and the results are reproducible. The conversion of ethanol is reported in Fig. 5 as function of temperature.

It is clearly shown that ethanol was not fully converted at 500 °C up to 600 °C in the absence of catalyst. Ethanol was decomposed and ethylene and acetaldehyde were formed as the main products at 600 °C but ethanol conversion is much lower than 22%. Similar results were obtained when the reactor was loaded with pure HMS material. These results suggest that ethanol dehydration and dehydrogenation were the main reactions.

In presence of Ce–HMS samples, ethanol conversion started at ca. 400 °C and increased with temperature. At 400 °C the ethanol conversion is around 16% for samples up $R = 0.1$ and 18% and 20% for samples with $R = 0.2$ and 0.3. A very small part is decomposed in ethylene and acetaldehyde. Increasing the temperature, the thermal decomposition of ethanol becomes significant with ethylene and acetaldehyde being the main products. At 600 °C the ethanol conversion reach the 90% for samples up $R = 0.1$ and 93% and 95% for samples with $R = 0.2$ and 0.3 with an oxygen consumption of 87%.

The detected products after partial oxidation of bio-ethanol were hydrogen, methane, carbon dioxide, carbon monoxide, ethylene and acetaldehyde and carbon containing products. Indicated with CP*, they were diethyl ether, acetone and acetic acid. The product distribution as a function of temperature on a water-free basis for Ce–HMS samples with $R = 0.02$ and 0.3 is reported in Table 2.

The results evidence some difference in the quantity of detected product, and also suggest that a low cerium quantity can be used in this type of reaction. Generally, thermal decomposition of ethanol was observed as the first step of the reaction at 500 °C, and acetaldehyde was formed by ethanol dehydrogenation (Eq. (1)) and ethylene by ethanol dehydration (Eq. (2)). With increasing temperature ethanol conversion increased and product distribution changed. The quantity of the formed hydrogen and carbon monoxide increased at the expense of acetaldehyde.

$$CH_3CH_2OH \rightarrow C_2H_4O + H_2 \quad (1)$$

$$CH_3CH_2OH \rightarrow C_2H_4 + H_2O. \quad (2)$$

Ce–HMS materials, due to its acidic nature, promote the formation of ethylene by ethanol dehydration (Eq. (2)), which causes carbon deposits. At 600 °C, when ethanol conversion was 95–96%, quantity of acetaldehyde was lower but selectivity to ethylene was increased to around 44%.

Generally, ethylene is formed through a parallel route, with partial oxidation, in which catalytic sites of acidic nature present on the Ce–HMS domains play a significant role. The formation of H_2, CH_4, CO and CO_2 at 600 °C suggested that the ethanol decomposition is followed by acetaldehyde decomposition (Eq. (3)), and partial oxidation reactions, too.

$$C_2H_4O \rightarrow CH_4 + CO. \quad (3)$$

Ethylene formation can be prevented at 500–600 °C, thus reducing the possibility of coke formation if metals Pt, Pd or Ni are used as promoters. This will be the subject of the future work. Summarizing findings, Ce–HMS materials have interesting and perspective properties for catalytic application in reactions of reforming of ethanol. In principal, CeO_2, which is a material characterized by strong redox surface properties, promotes coke formation in the absence of oxygen by strong interaction with the adsorbed reaction intermediate species (aldehyde, ethoxides, etc.). The addition of oxides like CeO_2 to the silica support modified the acidic and textural properties of the matrix (HMS) and increased the dispersion and catalytic performances of supported promoters.

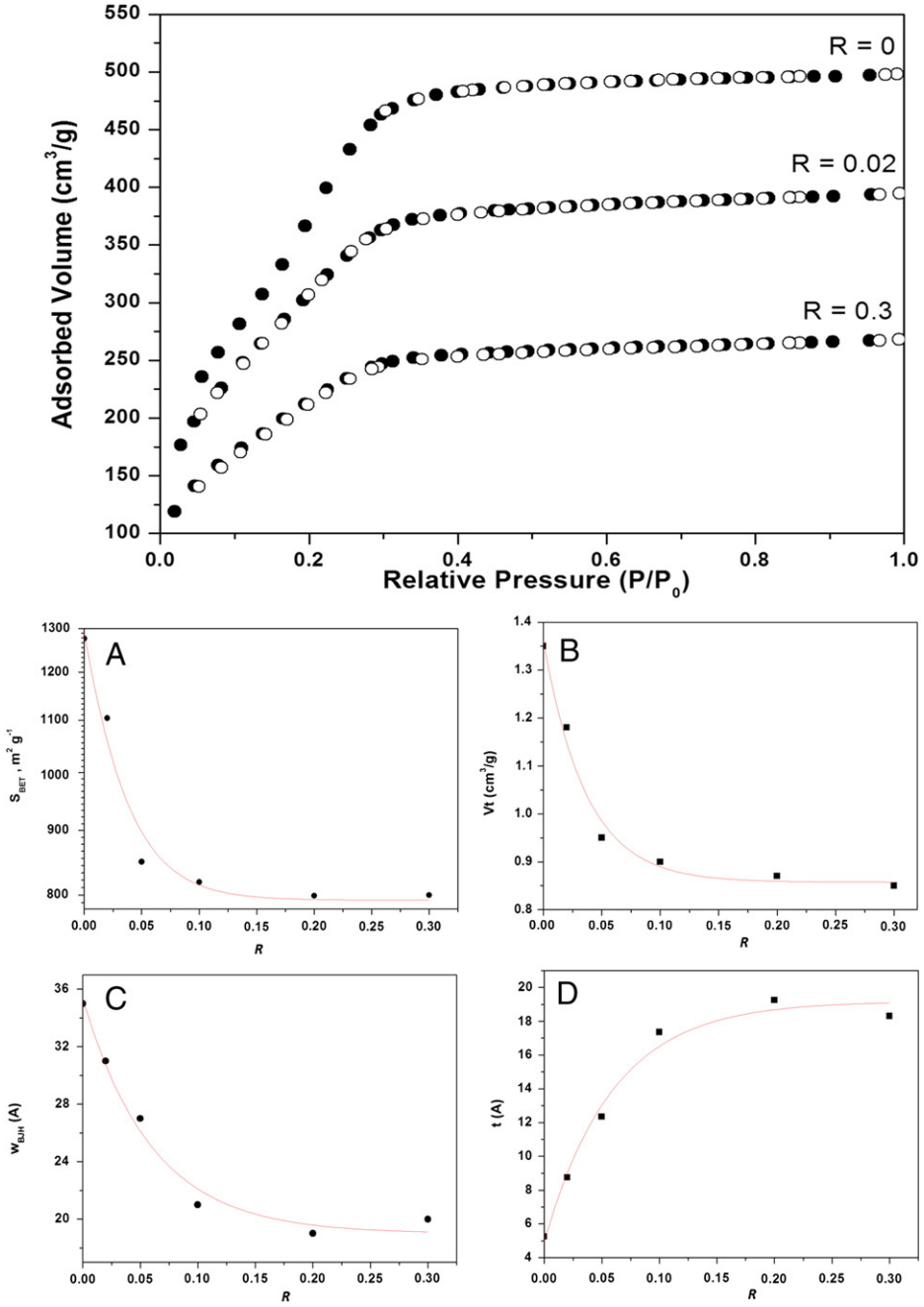

Fig. 3. Nitrogen adsorption–desorption isotherms of Ce–HMS samples. S_{BET}, V_t, w_{BJH} and t trend as function of R. The red lines are a guide for the eyes. (For interpretation of the references to color in this figure legend, the reader is referred to the web version of this article.).

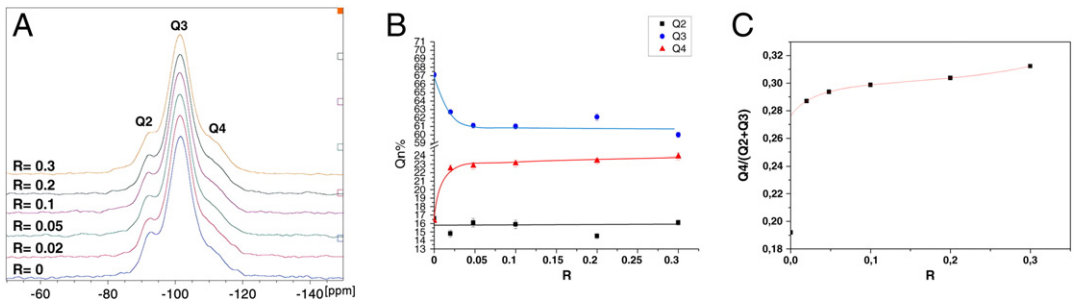

Fig. 4. A) ^{29}Si {^{1}H} CP–MAS NMR spectra of Ce–HMS samples. B)Peak areas obtained by deconvolution of the ^{29}Si {^{1}H} CP–MAS NMR area. C) Q4/(Q2 + Q3) ratio vs R.

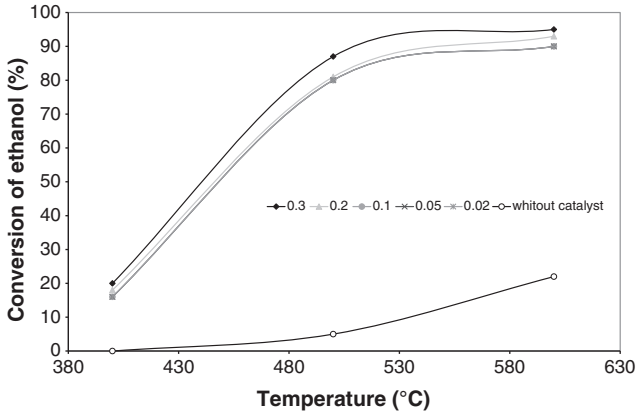

Fig. 5. Ethanol conversion in the partial oxidation over Ce–HMS samples at different temperatures (150 mg catalyst, 10 g/h ethanol, molar ratio oxygen/ethanol = 0.75).

Table 2
Percentage of detected products after partial oxidation of bio-ethanol conversion over Ce–HMS samples with $R = 0.02$ and 0.3 at T = 500 and 600 °C.

	$R = 0.02$		$R = 0.3$	
	T = 500 °C	T = 600 °C	T = 500 °C	T = 600 °C
Ethanol conversion	88.0%	96.0%	87.0%	95.0%
H_2	3.7%	5.0%	4.5%	6.0%
CO	35.0%	35.9%	34.0%	33.0%
CO_2	8.0%	5.6%	13.0%	10.3%
CH_4	5.7%	7.0%	4.0%	5.3%
C_2H_4	37.2%	44.8%	27.6%	41.9%
C_2H_4O	12.0%	4.0%	20.0%	8.0%
CP*	3.0%	2.0%	2.0%	2.0%

4. Conclusions

The incipient wetness method was used for the preparation of cerium oxide supported on HMS mesoporous silica. The hexagonal structure of HMS was maintained after the impregnation and cerianite particles are formed. The surface area and the pore diameter of the hexagonal structure decrease with the cerium quantity. At low quantity of cerium, cerianite particles are located inside the mesoporous channels. Increasing the quantity of cerium the cerianite is located inside and outside the channels, covering the HMS surface and partially obstructs the mesochannels.

Ce–HMS material is perspective material for catalytic application. Catalytic test in reaction of partial oxidation showed that ethanol conversion is influenced by reaction temperature. In addition, results showed that it is active with low quantity of cerium. It is a very important result considering the high cost of lanthanides and their low availability.

Acknowledgments

The authors would like to thank the MIUR for supporting this research through the PRIN 2009 prot. 2009WXXLY2_004 “Application of microwaves irradiation on some inorganic syntheses and on bioactive compound and essential oils extraction”. SAXS and NMR experimental data were provided by the Centro Grandi Apparecchiature - UniNetLab - Università di Palermo funded by the P.O.R. Sicilia 2000–2006, Misura 3.15 Azione C Quota Regionale.

References

[1] C.T. Kresge, M.E. Leonowicz, W.J. Roth, Nature 359 (1992) 710.
[2] H. Yokoyama, Science 256 (1992) 66.
[3] Z.-Y. Yuan, H.-T. Ma, Q. Luo, W. Zhou, Materials Chemistry and Physics 77 (2002) 299–303.
[4] P. Oliveira, et al., Catalysis Letters 114 (2007) 192–197.
[5] K. Kili, F. Le Normand, Journal of Molecular Catalysis A: Chemical 140 (1999).
[6] R. Burch, T.C. Watling, Applied Catalysis 11 (1997) 207.
[7] K. Mohamed, S. Khalil, Journal of Colloid and Interface Science 315 (2007) 562–568.
[8] K.M.S. Khalil, Journal of Colloid and Interface Science 315 (2007) 562–568, (and references therein).
[9] S. Vetrivel, A. Pandurangan, Journal of Molecular Catalysis A: Chemical 227 (2005) 269–278.
[10] L.F. Liotta, G. Pantaleo, F. Puleo, A.M. Venezia, Catalysis Today 187 (2012) 10–19.
[11] W. Wang, Zh. Wang, Y. Ding, J. Xi, Catalysis Letters 81 (2002) 63–68.
[12] A. Haryanto, S. Fernando, N. Murali, S. Adhikari, Energy & Fuels 19 (2005) 2098–2106.
[13] L.V. Mattos, F.B. Noronha, Journal of Power Sources 152 (2005) 50–59.
[14] A.M. Silva, L.O.O. Costa, A.P.M.G. Barandas, L.E.P. Borges, L.V. Mattos, F.B. Noronha, Catalysis Today 133–135 (2008) 755–761.
[15] C.P. Rodrigues, V. Teixeira da Silva, M. Schmal, Applied Catalysis B: Environmental 96 (1–2) (2010) 1–9.
[16] A. Corma, Chemical Reviews 97 (1997) 2373–2419.
[17] M.L. Saladino, A. Spinella, E. Caponetti, A. Minoja, Microporous and Mesoporous Materials 113 (2008) 490–498.
[18] R.A. Young, The Rietveld Method, University Press, Oxford, 1993.
[19] L. Lutterotti, S. Gialanella, Acta Materialia 46 (1998) 101.
[20] S.R. Hartmann, E.L. Hahn, Physical Review 128 (1962) 2042.
[21] B.Ch. Enger, R. Lodeng, A. Holmen, Applied Catalysis A: General 346 (2008) 1–27.
[22] Wenju Wang, Yaquan Wang, International Journal of Hydrogen Energy 33 (2008) 5035–5044.
[23] P.T. Tanev, T.J. Pinnavaia, Science 267 (1995) 865–867.
[24] S.J. Gregg, K.S.W. Sing, Adsorption, Surface Area and Porosity, 2nd edition Academic Press, London, 1982.
[25] S. Brunauer, P.H. Emmett, E. Teller, Journal of the American Chemical Society 60 (1938) 309.
[26] M. Kruk, V. Antchshuk, M. Jaroniec, A. Sayari, The Journal of Physical Chemistry. B 103 (103) (1999) 10670.
[27] M. Kruk, M. Jaroniec, Y. Sakamoto, O. Terasaki, R. Ryoo, C.H. Ko, The Journal of Physical Chemistry. B 104 (2000) 292.